IOP Publishing Journal of Physics D: Applied Physics
J. Phys. D: Appl. Phys. **40** (2007) R319–R336 doi:10.1088/0022-3727/40/19/R01

TOPICAL REVIEW

Microfluidic methods for generating continuous droplet streams

G F Christopher and S L Anna

Department of Mechanical Engineering, Carnegie Mellon University, Pittsburgh, PA 15213 USA

E-mail: sanna@cmu.edu

Received 2 August 2007
Published 21 September 2007
Online at stacks.iop.org/JPhysD/40/R319

Abstract
Microfluidic technologies have emerged recently as a promising new route for the fabrication of uniform emulsions. In this paper, we review microfluidic methods for synthesizing uniform streams of droplets and bubbles, focusing on those that utilize pressure-driven flows. Three categories of microfluidic geometries are discussed, including co-flowing streams, cross-flowing streams, and flow focusing devices. In each category we summarize observations that have been reported to date in experiments and numerical simulations. We describe these results in the context of physical mechanisms for droplet breakup, and simple theoretical models that have been proposed. Applications of droplets in microfluidic devices are briefly reviewed.

1. Introduction

An emulsion contains liquid droplets suspended in a second immiscible liquid. The droplets are deformable, which imparts unique flow characteristics to the emulsion, including viscosity that changes with shear rate, and elasticity arising from surface tension [1]. The rheology, or flow behaviour of the emulsion is directly related to the texture we associate with skin lotion, mayonnaise, ice cream and a host of other foods and personal care products. The compartmentalization of liquids within droplets is also useful for controlling reactions, since the droplet interface acts as a membrane confining the contents. Using this concept, emulsions have been used to refine biochemical processes such as polymerase chain reaction (PCR) for gene analysis and to control drug delivery rates [2]. All of these important emulsion properties depend strongly on the suspended droplet size and the uniformity of sizes within the sample. Although numerous emulsification processes exist, most result in broad size distributions. Microfluidic technologies have recently emerged as a promising new route to the fabrication of uniform emulsions. In this paper, we review microfluidic methods for synthesizing uniform streams of droplets and bubbles, and we highlight unique features of microfluidic technologies that enable the development of novel applications.

Emulsions typically contain droplet diameters ranging from hundreds of nanometers to tens of micrometres. Microfluidic devices have similar geometric length scales, in the range of 10–100 micrometres. Microfluidic approaches to droplet formation are successful in part because these length scales are comparable. In addition, small length scales lead to low Reynolds number flows, in which fluid streams are laminar and easily controlled. Large surface area to volume ratios also lead to an increased role of surface effects. Over the past two decades, these unique characteristics have led to a dramatic increase in the development of novel applications exploiting the benefits of miniaturization [3, 4]. In droplet formation, the ability to control the local flow field via fabrication of complex microscale geometries enables control over the deformation and breakup of every individual droplet. The majority of microfluidic methods produce droplet diameters ranging from a few micrometres to hundreds of micrometres in a uniform, evenly spaced, continuous stream. Polydispersity, defined as the standard deviation of the size distribution divided by the mean droplet size, can be as small as 1–3%. Droplet volumes range from femtolitres to nanolitres.

Microfluidic methods for forming droplets can be either passive or active. Most methods are passive, relying on the flow field to deform the interface and promote the natural growth

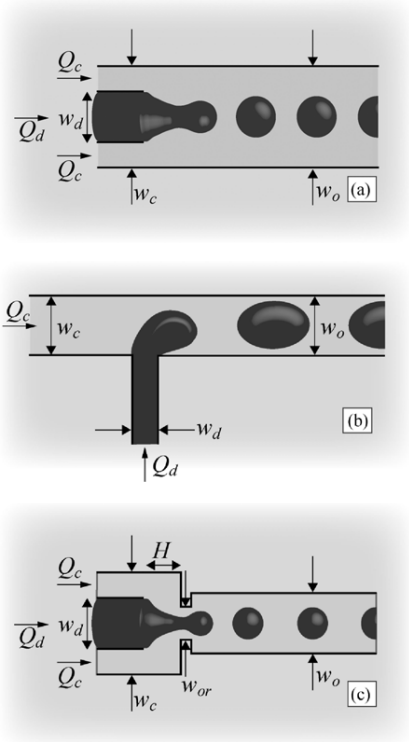

Figure 1. Illustrations of the three main microfluidic geometries used for droplet formation. (*a*) Co-flowing streams, (*b*) cross-flowing streams in a T-shaped junction, and (*c*) elongational flow in a flow focusing geometry. In each case the widths of the inlet and outlet streams are indicated. It is assumed that the device is planar with a uniform depth h.

of interfacial instabilities. These methods avoid moving parts and explicit external actuation. Passive methods can be grouped into three categories, characterized by the nature of the flow field near pinchoff: (1) breakup in co-flowing streams, (2) breakup in cross-flowing streams and (3) breakup in elongational or stretching dominated flows. Schematic illustrations of these three geometries are shown in figure 1. In general, the fluid phase to be dispersed is driven into a microchannel via a pressure-driven flow in which either volume flow rate or applied pressure are controlled. A second immiscible liquid is driven into a separate microchannel via an independently controlled flow. The two streams meet at a junction, at which the dispersed phase liquid extends to form a 'finger' or 'jet'. The geometry of the junction and the volumetric flow rates of the two fluids determine the local flow field, which deforms the interface. Eventually, a droplet pinches off from the dispersed phase finger by a free surface instability. Images depicting typical droplet breakup events in the three main microfluidic geometries are shown in figure 2. Steady flow of the two liquids yields periodic formation of equal-size droplets in a continuous stream. Generically, droplet breakup can be characterized by the competition between local fluid stresses acting to deform the liquid interface and capillary pressure acting to resist deformation. In addition, the emerging droplet obstructs the junction as it grows, leading to a dramatic increase in the upstream pressure, which also drives pinchoff. The wettability of the nearby channel walls is critically important to the process, determining which liquid phase is dispersed.

In comparison with conventional methods, microfluidic technologies for droplet formation yield considerably more control over the droplet size and the uniformity. For example, high-energy methods such as atomization, sprays, and high-speed mixing yield broad size distributions due to stochastic processes such as turbulent fluctuations. Pore-based methods such as membrane emulsification [5], microchannel emulsification [6, 7], and related methods [8–10] force the two immiscible liquids together through a filter or a microfabricated array of pores. Here, droplet size distribution can be significantly narrower, but the pore size distribution limits the uniformity of the resulting emulsion. Inkjet printing is an example of a well-developed microtechnology in which droplets fragment from a liquid jet emitting from a capillary or a nozzle [11, 12]. This method allows for the formation of very uniform streams, although the formation of secondary satellite droplets must be controlled. External actuation of the nozzle head is one method for tuning satellite formation, and it also enables the ejection of a single droplet at a time [13–15]. Several additional novel droplet formation methods have been developed recently that offer substantial control over uniformity and size, including selective withdrawal [16], flow focusing [17, 18] and co-flowing a liquid past a capillary tube [19]. Each of these methods utilizes a specific flow field to promote the uniform breakup of a fine liquid thread. Some of these methods motivated the development of specific microfluidic geometries, and will be discussed in more detail later in this review.

While selective withdrawal and flow focusing offer a similar level of control over size and uniformity compared with microfluidic methods, microfluidics offers several additional advantages. As in any emulsion, the droplet interface encloses its contents, enabling droplets to act as convenient vessels for transporting materials and carrying out chemical reactions [2]. In microfluidics, the interface offers the significant added benefit of preventing sample dispersion and fouling of the channel walls. The ability to generate a wide range of precise volumes allows for control over stoichiometry or reactant inventories, and the ability to control downstream droplet velocities, sorting, coalescence and internal mixing allows the possibility of manipulating and imaging the spatial distribution of droplets for time-resolved kinetics studies [20, 21]. Finally, the entire process is miniaturized, enabling the rapid analysis of very small quantities of reagents in a portable, automated and inexpensive format [4]. These capabilities have led to the development of numerous applications that could not have been realized in other ways. Protein crystallization, advanced flow cytometry, enzyme kinetics studies, and DNA and blood analysis are examples of biotechnology applications that have been implemented in droplet-based microfluidic devices [21, 22]. In addition, droplets have been used as reactors for synthesizing materials with specific functionalities, including polymeric microparticles, metallic nanoparticles, colloid or lipid coated microcapsules and janus particles.

In this review, we describe recent microfluidic processes for generating continuous streams of uniform droplets. We emphasize passive methods, organizing these in terms of the local flow field used to break the droplets. Three

categories emerge: co-flowing streams, cross-flowing streams and elongation-dominated flows. In all cases, we consider closed microchannels in which the continuous phase liquid preferentially wets the walls. In principle, the droplet is prevented from contacting the wall due to an ever-present thin film of the surrounding liquid, and thus the influence of a three-phase contact line can be neglected. Wetting and capillary phenomena related to moving contact lines in microchannels are discussed more broadly in several recent reviews [23–25]. We also do not address the motion of droplets on open substrates, which can be induced by applied voltage or temperature gradients and form the basis of recent 'digital microfluidics' technologies [26]. In the following section, we introduce the key fluid forces and physical parameters important to microfluidic droplet formation processes. In section 3 we examine the mechanisms for droplet breakup in the three main categories of microfluidic breakup. External actuation methods are highlighted in section 4. Finally, section 5 highlights a few of the numerous applications of droplets in microfluidic devices.

2. Fundamentals of droplet breakup in microscale geometries

2.1. Experimental methods and physical parameters

Droplet formation in microfluidic devices utilizes independently controlled flows of two immiscible liquids. Most commonly, water or an aqueous solution is dispersed into a continuous phase of oil, or gas bubbles are dispersed into water. In general, the important fluid properties are the viscosities, μ_d and μ_c, the densities, ρ_d and ρ_c, and the interfacial tension σ. Throughout this review we will use the subscripts 'd' and 'c' to refer to the dispersed phase liquid and the continuous phase liquid, respectively. Liquids are typically Newtonian, with only a few studies examining the role of viscoelasticity on breakup [27, 28]. Pressure-driven flow is accomplished using either syringe pumps, which impose constant volumetric flow rates Q_d and Q_c, or gas pressure cylinders, in which a regulator controls the imposed pressures P_d and P_c.

The geometry of the microchannel junction determines the flow field that deforms the emerging liquid finger and pinches off a droplet. Lithography-derived processes are typically used to fabricate these complex geometries. In lithographic techniques, an arbitrary planar design is converted into a network of rectangular microchannels with uniform depth h. Soft lithography using flexible poly(dimethylsiloxane) (PDMS) or polyurethane-based polymers is one of the most popular methods, due to the ease and speed with which new designs can be prototyped [29]. Other popular methods etch channels in glass or silicon [30, 31]. The geometries used to generate droplets can be defined in terms of the depth h and the widths of the two inlet streams, w_d and w_c. The dimensions corresponding to each of the three main geometries are labelled in figure 1. The width of the outlet channel w_o into which the droplets travel after they break can also be specified. Additional geometric parameters needed to describe specific geometries are shown in figure 1 and defined in section 3. The lengths of the inlet and outlet channels are not typically reported, since it is assumed that the local flow field controls the droplet breakup dynamics. However, we note that the channel lengths determine the local absolute pressure in the device, since the pressure at each outlet is held fixed at atmospheric pressure.

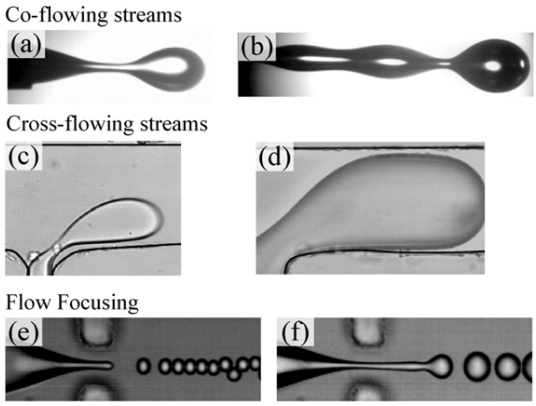

Figure 2. Images of droplet breakup in each of the three main microfluidic geometries used for droplet formation. Breakup in co-flowing streams is shown in (*a*) dripping and (*b*) jetting modes. (Reprinted from [48], Copyright 2004, with permission from Elsevier.) Breakup in cross-flowing streams is shown in (*c*) unconfined and (*d*) confined T-junction geometries [51]. Flow focusing geometries lead to breakup in elongational flows in (*e*) dripping and (*f*) jetting modes. (Reprinted with permission from [52], Copyright 2006, American Institute of Physics.)

To understand the dynamics of droplet breakup, we examine the local viscous stresses and the dynamic pressure field surrounding the emerging droplet. Viscous stresses due to the continuous phase liquid can be estimated by the product $\mu_c G$, where G is a characteristic rate of strain that is proportional to the outer flow rate Q_c and a geometric factor. Estimating the magnitude of G depends on the specific geometry, and will be described further in section 3. In addition to the viscous stress, the interfacial tension leads to a normal stress jump across the curved interface of the emerging droplet. The normal stress jump is proportional to the local interface curvature κ; in the absence of flow this leads to $(p_d - p_c) \sim \sigma\kappa$. The interface shape can be quite complicated, as shown in figure 2, such that estimates of κ vary both during the breakup process and in different parts of the growing droplet. Nevertheless, the curvature is bounded by the geometry. For example, the maximum radius in the depth direction is $r_c \sim 1/\kappa \sim h/2$. In the plane, the radius is initially comparable to the half width of the dispersed phase channel $w_d/2$. Later in the growth process, the protruding tip is limited to a maximum radius of $w_o/2$. Thus, the interface shape depends strongly on the particular geometry. As the droplet grows, it obstructs the channel, restricting the flow of continuous phase liquid around it. This reduction in the gap through which the continuous phase liquid can flow leads to a dramatic increase in the dynamic pressure in the continuous phase upstream of the droplet. The increased pressure drives the interface to neck and pinch into a discrete droplet. A lubrication analysis can be used to estimate the excess pressure due to the obstruction [32]. The form of the pressure term depends on the shape of the emerging finger that obstructs the flow.

Several key dimensionless parameters can be used to analyse the relative importance of each of the key forces

for droplet breakup. In microfluidic droplet formation, the capillary number Ca is the most important of these, characterizing the relative importance of viscous stresses and capillary pressure. We define the capillary number for microfluidic droplet formation in terms of the continuous phase flow field that acts to deform the droplet,

$$Ca = \frac{\mu_c G a}{\sigma} \propto \frac{\mu_c Q_c S a}{\sigma}, \tag{1}$$

where a is the characteristic size of the finger prior to entering the junction, S is a geometric factor, and G is the predominant elongational or shear rate-of-strain in the flow field. This definition is consistent with classic experiments examining the deformation and breakup of isolated droplets in linear flows [33], enabling comparison with these benchmark studies. In microfluidic droplet formation, capillary numbers typically range from $Ca \sim 10^{-3}$ to 10^{1} for flow rates accessible using syringe pumps.

An additional dimensionless parameter that is important in microfluidic droplet formation is the ratio of volumetric flow rates φ, given by

$$\varphi = Q_d/Q_c. \tag{2}$$

In the limit as $\varphi \to 0$, the dispersed phase liquid remains stationary, mimicking classic droplet dynamics experiments in a four roll mill apparatus [34]. Finally, the viscosity ratio λ, given by

$$\lambda = \mu_d/\mu_c, \tag{3}$$

also characterizes droplet breakup.

The Reynolds number Re indicates the importance of inertia compared with viscous stresses, and is defined in terms of the characteristic velocity U of the flow,

$$Re = \frac{\rho U D_H}{\mu} = \frac{2\rho_i Q_i}{\mu_i(w_i + h_i)}, \tag{4}$$

where D_H is the hydraulic diameter of the microchannel, and the subscript 'i' denotes the liquid phase under consideration. Small geometric length scales typically lead to $Re \ll 1$ for microfluidics.

The Weber number We is used frequently to parametrize droplet breakup processes when inertia and capillary pressure are more important than viscous stresses. The product of the Reynolds number and the capillary number gives the Weber number,

$$We = Re\, Ca. \tag{5}$$

Typically, inertia is the least important of the three key forces in microfluidics [3,4]; however, inertia does play a role in bubble collapse [35,36] and in nonlinear bubble formation at higher flow rates [28,37,38].

Finally, the Bond number Bo characterizes the relative importance of buoyancy and surface tension, and is given by

$$Bo = \frac{\Delta\rho g w^2}{\sigma}, \tag{6}$$

where $\Delta\rho = \rho_d - \rho_c$ is the density difference between the two immiscible fluids. For air bubbles in water, in a microchannel with $w = 100\,\mu$m, $Bo \sim 10^{-3}$. For water droplets in oil, the density difference is typically very small, and so the magnitude of Bo can be as much as a factor of a thousand smaller. Thus, buoyancy is typically negligible in droplet formation in microfluidic devices.

In the following sections, we utilize the above notation and definitions in an effort to facilitate comparisons between studies; however, we note that there is currently no standard, and readers will find alternatives in the cited literature.

2.2. Wettability and material selection

The selection of appropriate materials for fabrication of droplet-based microfluidic devices is essential. One key reason is that the wettability of the microchannel walls strongly influences droplet formation due to the proximity of the walls and the possibility for either liquid phase to encounter the wall. In order to achieve consistent droplet breakup, it is important that the continuous phase liquid preferentially wets the walls. For this reason, experimental protocols often involve 'priming' the microfluidic device by filling with continuous phase liquid to pre-wet the walls. If the continuous phase liquid wets much more readily than the dispersed phase liquid, then a thin liquid film will form between the droplet interface and the wall. If the two liquids wet the substrate comparably, erratic two-phase flow patterns are observed [39,40], and uniform droplet production is compromised. Dreyfus *et al* present a scaling argument suggesting that competitive wetting becomes more important the smaller the channel [39].

These observations show that wettability of the substrate is the controlling factor in determining the morphology of the resulting emulsion. For example, since PDMS is hydrophobic, most droplet breakup studies in which devices are fabricated using soft lithography are limited to the formation of water droplets surrounded by oil. Oil droplets in water can be generated by fabricating in silicon, which is hydrophilic [41], by using concentrated surfactant solutions to alter the relative wettability of the two liquids [42], by using a modified 'laser LIGA' method to fabricate channels from PMMA plastic [30], and by fabricating three-dimensional geometries to minimize contact of the dispersed phase liquid with the walls [43,44]. Furthermore, Xu *et al* [40] argue that using concentrated surfactant solutions can result in the formation of a surfactant monolayer on the microchannel walls, altering the surface to promote wetting of the surfactant solution.

Material selection is also important from the perspective of compatibility with solvents and strength of materials. PDMS, though ubiquitous, is not compatible with many solvents of interest since it swells or degrades in these solvents. A few studies have demonstrated successful droplet formation in microfluidic devices fabricated using alternative materials that are stable to a wider range of solvents [45,46]. Fabrication in materials such as silicon and glass and fabrication of three-dimensional monolithic structures can yield devices that withstand higher pressures without failure and allow increased throughput [43,44,47].

3. Passive microfluidic methods

3.1. Droplet breakup in co-flowing streams

The simplest microfluidic geometry for achieving droplet formation is a set of concentric channels, where the dispersed phase liquid is driven into the inner channel or capillary, and emerges from the end of the capillary into a parallel flowing stream of the continuous phase liquid. This configuration is depicted schematically in figure 1(*a*) and it has been implemented at the macroscale by Umbanhowar *et al* [19].

In this study, a micropipette is inserted into a rotating bath of the continuous phase liquid [19]. The authors demonstrate that the rotating bath configuration generates emulsions using many different liquid pairs. Cramer *et al* [48] implemented co-flowing streams in a slightly different way, by inserting a microcapillary (I.D. 100 μm) into a rectangular flow cell measuring 20 mm × 2.5 mm. They also examined a microfluidic equivalent of the same configuration, in both cases using oil as the continuous phase liquid. The influence of viscosity ratio was investigated using aqueous solutions of κ-carrageenan as the dispersed phase liquid, and varying the concentration of dissolved κ-carrageenan from 0.1 to 1.5 wt% in order to alter the viscosity. Although aqueous solutions of κ-carrageenan shear thin, the authors assumed the effect has a negligible impact on their experiments.

Droplet breakup from a capillary tip immersed in a continuous co-flowing liquid can be separated into two distinct breakup regimes: dripping, in which droplets pinch off near the capillary tip, and jetting, in which droplets pinch off from an extended thread downstream of the capillary tip [48]. Typical images of droplets forming in each of these modes are shown in figures 2(*a*) and (*b*). The transition from dripping to jetting occurs as the continuous phase velocity increases above a critical value. Cramer *et al* found that the critical velocity decreases as the dispersed phase flow rate increases, due to the larger axial momentum of the forming droplet, facilitating jet formation. The critical velocity also decreases as the dispersed phase viscosity increases, due to enhanced stability of the liquid–liquid interface. Finally, the critical velocity decreases with reduced interfacial tension, since the interfacial tension is the primary force acting to hold the emerging droplet at the capillary tip. The existence of these two distinct modes of breakup as well as the dependence of the transition on the key dimensionless parameters was predicted by Zhang and Stone [49] using boundary integral simulations. A more recent, general stability analysis of viscous threads confined within a viscous outer liquid in a microchannel characterizes the transition from droplet to jet formation as a transition from an *absolute* to a *convective* instability, in which the faster flow of the outer liquid and the confinement allow a stable thread to form prior to pinchoff of larger droplets [50]. In this paper, Guillot *et al* analyse the transition in detail as a function of viscosity ratio, capillary number and 'confinement', in which the confinement parameter $x = r_{\mathrm{jet}}/R_{\mathrm{c}} = f(\lambda, \varphi)$ is defined in terms of the size of the jet relative to the effective radius of the channel, which is a function of both viscosity ratio and flow rate ratio. The predicted transitions are found to agree well with the experimental observations.

In both the rotating bath and the rectangular flow cell configurations, the droplet size has been characterized as a function of the control parameters. In general, droplets are smaller when the continuous phase velocity is faster, due to larger shear stresses exerted on the interface. Droplet size generally increases with increasing dispersed phase flow rate. An emerging droplet continues to fill during pinchoff, so a larger internal flow rate leads to more volume entering a droplet prior to pinchoff. These trends were observed by Cramer *et al* [48] who performed quantitative measurements of droplet size, polydispersity and droplet formation time, systematically varying the relevant physical parameters. While the most detailed measurements were conducted within the dripping regime, droplet sizes are also reported for the jetting regime, and the data in both regimes show similar trends. In the experiments, droplet diameter decreases monotonically with increasing continuous phase velocity. Reducing the interfacial tension results in larger droplets due to decreased resistance to breakup. On the other hand, variations in viscosity ratio have little effect on droplet size over a wide range of continuous phase velocities. The authors also report that droplet formation time decreases with increasing dispersed phase flow rate for a fixed continuous phase velocity, and approaches a constant value at small continuous phase velocities. Umbanhowar *et al* [19] also measured droplet size, and compare the experimental data with a scaling model derived from a force balance on the growing droplet. The predicted droplet size is obtained by finding the roots of the nondimensional equation

$$\bar{d}^3 - \left(1 + \frac{1}{3Ca}\right)\bar{d}^2 - \frac{\varphi}{\alpha}\bar{d} + \frac{\varphi}{\alpha} = 0, \tag{7}$$

where $\bar{d} = d/d_{\mathrm{i}}$ is the droplet size scaled by the inner diameter of the capillary tube, and the capillary number in this case is defined in terms of the velocity of the continuous phase liquid U_{c}, $Ca \equiv \mu_{\mathrm{c}} U_{\mathrm{c}}/\sigma = \mu_{\mathrm{c}} Q_{\mathrm{c}}/\sigma A_{\mathrm{c}}$, with A_{c} denoting the cross-sectional area of the outer channel. The ratio of velocities is given by α/φ, where $\alpha = A_{\mathrm{d}}/A_{\mathrm{c}}$ is the ratio of the two cross-sectional areas and φ is the flow rate ratio that we have previously defined. We note that the predicted droplet size is independent of the dispersed phase viscosity, consistent with the experiments in [48]. Umbanhowar *et al* deliberately avoid the jetting regime in experiments, and argue that dripping will occur when the capillary pressure is more important than inertia, $We < 1$, or when the internal flow rate remains below the limit, $Q_{\mathrm{d}} < \pi(d^3\sigma/2\rho_{\mathrm{d}})^{1/2}$. Furthermore, the authors point out that as long as the internal flow rate is slow enough, the above equation reduces to

$$\bar{d} \approx 1 + \frac{1}{3Ca}. \tag{8}$$

The experimental results agree well with the predicted values over the range of experiment conditions considered, validating the assumption that viscous stresses and capillary pressure are the leading factors in droplet breakup. Both of the co-flowing configurations described here result in highly monodisperse droplets with polydispersity values ranging from 1% to 2%. The droplet sizes produced range from as small as 80 μm up to a few hundred micrometres in diameter.

3.2. Droplet breakup in cross-flowing streams

One of the most common microfluidic methods of generating droplets uses cross-flowing continuous and dispersed phase streams. In microfluidics, this is typically implemented using T-shaped microchannel junctions, depicted schematically in figure 1(*b*). Droplet formation in a T-shaped device was first reported by Thorsen *et al* [53], who used pressure controlled flow in microchannels 35 μm wide and 6.5 μm deep to generate droplets of water in a variety of different oils. When the imposed pressures are comparable, $P_{\mathrm{d}} \sim P_{\mathrm{c}}$, the droplet size increases with increasing dispersed phase pressure P_{d}.

Droplets do not form when the pressures are significantly different from each other. For example, if the dispersed phase pressure is significantly smaller than the continuous phase pressure P_c, the liquid interface cannot enter the junction region. Conversely, when P_d is much larger than P_c, the two streams co-flow downstream and the interface remains stable. The authors propose a simple argument based on the original work of Taylor [54] that droplets should pinch off when the viscous stresses overcome the interfacial tension, or $Ca \sim 1$, leading to the expression for the droplet diameter,

$$d \sim \frac{2\sigma}{\mu_C \dot{\varepsilon}}, \tag{9}$$

where $\dot{\varepsilon}$ is the shear rate within the junction. This simple argument predicts droplet sizes within a factor of two of the measured sizes, although it is necessary to obtain shear rate values empirically, and the relationship between $\dot{\varepsilon}$, P_c and P_d is not clear.

Following this initial work, a number of studies have examined the characteristics of droplet breakup in microfluidic T-junctions. This geometry is popular due to the ease with which droplets can be formed and the uniformity of the resulting droplets. Over a wide range of flow rates, the droplet formation is periodic and regular as long as a single T-shaped channel is used. On the other hand, recent studies report that droplet and bubble breakup is not necessarily regular when multiple droplet generators are coupled via a single set of syringe pumps [55, 70]. The interaction between multiple breakup processes leads to a rich nonlinear dynamics in which droplet formation can appear uniform, multi-modal or chaotic.

Most T-junction studies fall into one of two groups: those in which the emerging droplet rapidly fills the junction region and is influenced by its confinement within the microchannel, and those in which the emerging droplets do not interact with the downstream microchannel walls and remain unconfined by the microchannel. Images representing typical droplet shapes during breakup in confined and unconfined geometries are shown in figures 2(*c*) and (*d*). Unconfined droplets do not disrupt the continuous phase flow significantly, and thus their size is primarily controlled by the local shear stress. Confined droplets restrict the flow of the continuous phase liquid to the thin film between the liquid interface and the microchannel walls. This obstruction leads to increased upstream pressure in the continuous phase liquid, driving pinching of the interface. Nominally, unconfined breakup occurs when the width of the continuous phase channel is much larger than that of the dispersed phase channel. It is likely that both the pinching pressure and the shear stress are important for many microfluidic flow conditions, and this 'mixed' case has been considered in a recent numerical study using a phase field model [56], as well as experimentally [51]. Since most studies emphasize either confined or unconfined droplet breakup, we will use this classification in summarizing the current literature on microfluidic droplet generation due to cross-flow.

3.2.1. Unconfined droplet breakup in cross-flowing streams. Several studies examine the mechanisms for droplet breakup in cross-flowing streams in which the width of the continuous phase channel is much greater than that of the dispersed phase channel. In studies using planar microfluidic channels, channel dimensions range from 25 to 500 μm, and the width of the continuous phase channel is at least a factor of five larger than that of the dispersed phase channel [27, 30, 57]. The depth of the microchannel is usually smaller than the width of either channel. In a separate study, Xu *et al* [58] connected a 45 μm square microchannel to a relatively large 1 mm square chamber in order to minimize the influence of confinement. Droplets were generated in these systems using both water and oil as the dispersed phase liquids, depending on the wetting properties of the devices used. The droplet sizes observed in these studies ranged from 100 to 800 μm in size. In all cases, the droplet size decreases as the speed of the continuous phase liquid increases, for a fixed internal flow speed. The dependence of the droplet size on the dispersed phase flow rate is less consistent, although most studies report that the droplet size increases at least weakly with increasing dispersed phase flow rate. A few studies specifically examine the influence of the liquid viscosities [27] and the interfacial tension [58] on breakup. Xu *et al* report that the droplet size approaches a minimum value at large continuous phase velocities, independent of the magnitude of the dispersed phase velocity.

Simple models for the droplet size have been presented by Husny and Cooper-White [27] and by Xu *et al* [58]. Both models derive from a balance of forces on the emerging, unconfined droplet. Husny and Cooper-White argue that droplet breakup should occur when the drag exerted on the emerging droplet by the cross-flowing continuous phase liquid overcomes the interfacial tension resisting deformation of the droplet. Re-casting the expressions given by the authors in the notation defined earlier and collecting terms, the droplet size predicted from this force balance is given by

$$\bar{d}^4 - 2\bar{d}^3 + \frac{\psi}{2}\bar{d}^2 + \frac{\alpha}{2C_\lambda Ca} = 0, \tag{10}$$

where $\bar{d} = d/D_c$ is the droplet diameter scaled by the hydraulic diameter of the continuous phase channel, $D_c = 2w_c h/(w_c + h)$. In this case the capillary number is given by $Ca = \mu_c Q_c/\sigma w_c h$, the parameter $\alpha = (w_d/D_c)^2$ is a ratio of effective areas of the two channels, analogous to that defined in equation (7) for co-flowing streams, and $C_\lambda = (3 + 2/\lambda)/(1 + 1/\lambda)$ is a correction factor accounting for the viscosity ratio λ. The constant ψ represents the ratio of the droplet velocity to the average velocity of the continuous phase liquid. This value ranges from $0 < \psi < 2$ and depends on the capillary number; however, Husny and Cooper-White treat ψ as a fitting parameter with a constant value of $\psi = 0.6$ for their experiments. We note that equation (10) indicates that the droplet size resulting from unconfined breakup in cross-flowing streams should depend solely on the capillary number. The predicted droplet size is independent of the flow rate ratio, and it agrees with measured droplet sizes obtained from experiments to within 25% over the range of experiment conditions, as shown in figure 3(*a*) which shows nondimensional droplet diameter as a function of capillary number. Glycerol–water mixtures were used to tune the viscosity of the dispersed phase liquid, and the resulting measurements appear to be independent of the viscosity ratio to within the accuracy of the measurements. Discrepancies between the predicted and the

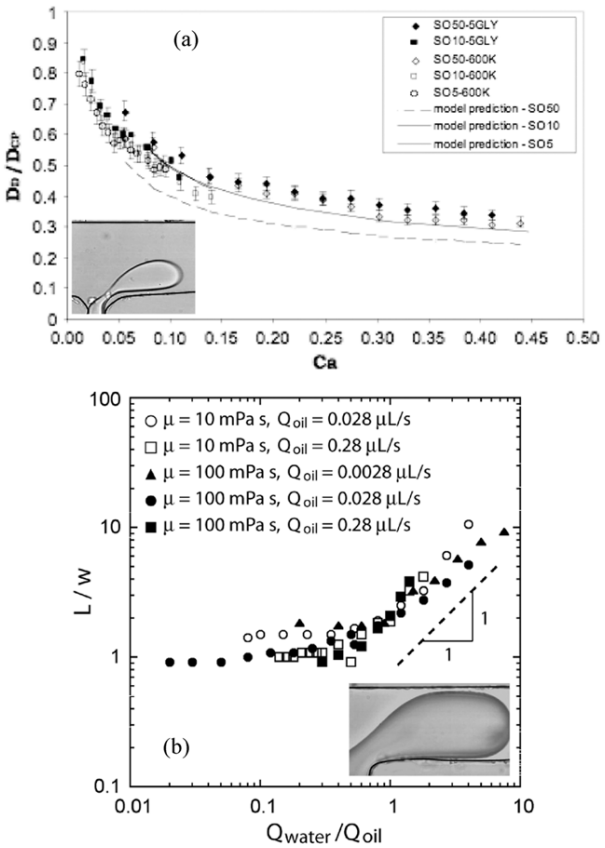

Figure 3. Graphs depicting dependence of droplet size on flow parameters in (*a*) unconfined breakup (reprinted from [27], Copyright 2006, with permission from Elsevier), and (*b*) confined breakup in a T-junction (reproduced from [59] by permission from The Royal Society of Chemistry). In the unconfined case, droplet diameter depends only on the capillary number. In the confined case, droplet length depends only on the flow rate ratio.

experimental droplet sizes are likely due to the choice of a constant value of ψ to characterize the relative velocity of a wide range of droplet sizes. At large values of the capillary number, the droplet size approaches a constant value of $\bar{d} = 0.3$. The authors argue that this limiting value is a function of the dispersed phase viscosity, although conclusive data are not shown. Nonetheless, this simple model captures the complex dynamics of droplet breakup over a wide range of capillary numbers.

Xu *et al* argue that additional forces should be included for their cross-flow configuration. In addition to the cross-flow drag analogous to that considered by Husny and Cooper-White, the authors included a dynamic lift force and buoyancy, in part because they considered a larger range of Reynolds numbers than the microfluidics studies. Re-casting the torque balance given in [58] in terms of our previously defined notation, a prediction for the droplet size is obtained,

$$[5.481\alpha Re^{1/2}Ca + Bo/6]\bar{d}^4 + 6Ca\bar{d}^3 - \bar{d} + 1 = 0, \quad (11)$$

where $\bar{d} = d/w_d$ is the droplet diameter scaled by the width of the microchannel screen hole. The capillary number is given by $Ca = \mu_c Q_c/\sigma w_c h$, the Reynolds number is given by $Re = \rho_c Q_c/\mu_c h$ and the Bond number is given by $Bo = \Delta\rho g w_d^2/\sigma$. The parameter $\alpha = (w_d/w_c)^2$ is the ratio of the effective cross-sectional areas of the two streams. The predicted diameter agrees well with the measured values for larger values of surface tension, but slightly under predicts the measured diameters for lower surface tension values. The authors argue that this discrepancy arises from the observation of an extended droplet detachment time subsequent to droplet growth as surface tension is reduced. Longer detachment times result in larger drops than predicted since more time is available for the fluid to enter the droplet prior to detachment. The authors argue that the detachment time is important when the drag force is smaller than the capillary force, or when the ratio x falls below a critical value, given by

$$x = \frac{F_D d}{F_C w_d} = \frac{3Ca\bar{d}^3}{(\bar{d} - 1)} < 0.9, \quad (12)$$

where F_D is the viscous drag and F_C is the capillary force resisting detachment. The critical value of $x < 0.9$ is based on conditions at which discrepancies between model and experiment became significant. Empirically, the detachment time t_d was found to depend on x in the following way:

$$\log(t_d) = 7.75 - 9.785x \quad (13)$$

The product $Q_d t_d$ represents the extra volume entering the droplet prior to detachment; equation (13) provides a means of empirically adjusting the predicted size from equation (12) [58, 60].

Regardless of the particular geometry used, droplet breakup in a cross-flowing stream is primarily controlled by the viscous drag when the droplets emerge from the capillary into a relatively wide stream. Although all experiments show that droplet size depends strongly on the continuous phase flow speed and only weakly on the dispersed phase flow speed, the proposed models appear to be specific to the particular geometry considered, and to rely on empirical fits to experimental data as inputs to the model.

3.2.2. Confined droplet breakup due to cross-flowing streams. Confined breakup occurs when the emerging droplet grows large enough to completely obstruct the continuous phase channel apart from a thin film of liquid surrounding the emerging droplet. Droplets created under these conditions are often referred to as 'plugs' because the droplet fills the channel cross-section, and its length in the flow direction is greater than its width. Due to the obstruction of the continuous phase channel by the plugs, the upstream pressure in the continuous phase liquid increases, resulting in an additional force exerted on the interface that promotes breakup.

Numerous experimental studies have examined the sizes of plugs formed in T-shaped microchannels over a range of flow conditions [59–61]. In these T-shaped devices, the widths of the dispersed and continuous phase channels are comparable to or equal to one another, as well as to the channel depth. Water is most frequently used as the dispersed phase liquid, and a variety of oils are used as continuous phase liquids, including perfluorooctanol and silicone oils ranging in viscosity from 10 to 100 mPa s. Flow conditions span a wide range of continuous phase flow rates, up to a capillary number of $Ca = \mu_c U_c/\sigma = \mu_c Q_c/\sigma w_c h < 0.1$, and over four orders of magnitude in flow rate ratio $\varphi = Q_d/Q_c$. Measured plug lengths range

in size from $L \sim 100$ to 350 μm ($1 < L/w_c < 10$, $w_c > h$). In all the reported experiments, the plug size is consistently independent of the cross-flowing continuous phase flow rate, or capillary number, while plug sizes increase as the flow rate ratio increases for fixed capillary number.

Garstecki *et al* [59,65] argue generally that at low capillary numbers a plug obstructing the continuous phase channel results in a significant increase in the flow resistance in the thin film region surrounding the droplet. The resulting increased pressure upstream 'squeezes' the neck of the droplet until it thins and breaks. The added force due to the pinching pressure scales with the distance ε between the emerging droplet and the outer wall,

$$F_p \approx \frac{\mu_c Q_c w_c}{h^2 \varepsilon^3}. \tag{14}$$

As droplets grow larger, the gap ε decreases and the pinching pressure exceeds the viscous shear stress, which only scales with $1/\varepsilon^2$. The authors argue that plugs formed at low capillary numbers grow until they block the channel, at which point the pressure force begins to squeeze the neck. The droplet continues to grow during this time. Assuming that the neck squeezes at a rate proportional to the average velocity of the continuous phase liquid, and that the plug fills at a rate proportional to the volumetric flow rate of the dispersed phase liquid, a scaling law for the final length L of the plug is obtained,

$$\bar{L} = L/w_c = 1 + \alpha\varphi, \tag{15}$$

where α is a constant factor related to the width of the thinning neck. Equation (15) clearly shows that plug lengths formed at low capillary number depend only on the flow rate ratio and not on the capillary number, consistent with experiments. Measured plug lengths agree well with the scaling law given in equation (15) when the factor α is unity, as shown in figure 3(*b*) which shows nondimensional droplet diameter as a function of capillary number. Garstecki *et al* argue that the above relationship is valid as long as the width of the dispersed phase channel w_d is greater than half the width of the continuous phase channel w_c. For smaller values of w_d, the shear stress on the emerging droplet will significantly distort its shape and will influence the final droplet size. A recent numerical study expands on the idea that both the 'pinching pressure' and the shear stress are significant above a critical value of the capillary number, and this mixture of the two forces leads to droplet breakup regimes analogous to dripping and jetting regimes observed in the other two geometries discussed in this review [56]. In this numerical study, de Menech *et al* demonstrate that the dripping regime in confined T-shaped junctions is qualitatively different from that observed in unbounded flows since the confinement pressure is never negligible. The study presents a detailed numerical exploration of the phase space defined by controllable parameters, and among other things demonstrates that the viscosity ratio plays an important role in the droplet formation, in contrast to expectations for unconfined breakup.

Van der Graaf *et al* [60] recently presented a semi-empirical model based on arguments similar to those of Garstecki *et al* [59]. The authors use the lattice Boltzmann method to simulate droplet breakup and perform experiments observing droplet growth and breakup. Based on simulations and experiments, the authors observe that in both confined and unconfined droplet breakup, droplet growth occurs in a two-step process. Initially, the droplet grows to a critical volume V_c until the forces exerted on the interface balance. Subsequently, the droplet continues to grow for a time t_n while the neck collapses, due to the influx of dispersed phase liquid, such that the final droplet volume is given by

$$V = V_c + t_n Q_d. \tag{16}$$

Furthermore, droplet volumes extracted from simulations decrease as capillary number increases and increase slightly as dispersed phase flow rate increases, consistent with other experimental observations reported for droplet breakup in cross-flowing streams. An empirical relationship is obtained, given by

$$V = V_{c,ref} Ca^m + t_{n,ref} Ca^n Q_d, \tag{17}$$

where $V_{c,ref}$ and $t_{n,ref}$ are taken from simulation results at $Ca = 1$, in which necking of the droplet is rapid. The exponents m and n depend on the device geometry, and are taken to be $m = n = 0.75$ in [60]. This empirical model works well for both confined plugs and unconfined droplets since the necking time increases as capillary number decreases, enhancing the influence of the dispersed phase flow rate.

In confined droplet breakup, droplets form within a specific range of flow parameters. In particular, as the flow rate ratio φ approaches unity, the liquid velocities become more similar, and it is generally observed that the two incoming streams co-flow downstream of the junction without pinching. Guillot and Colin [62] recently developed a semi-empirical model, supported by experiments, to describe the transition from droplets forming at a T-junction to stable parallel streams. A phase diagram depicting the observed transitions is shown in figure 4. The predicted transition depends primarily on the flow rate ratio and derives from the assumption that the upstream pressure drives pinchoff.

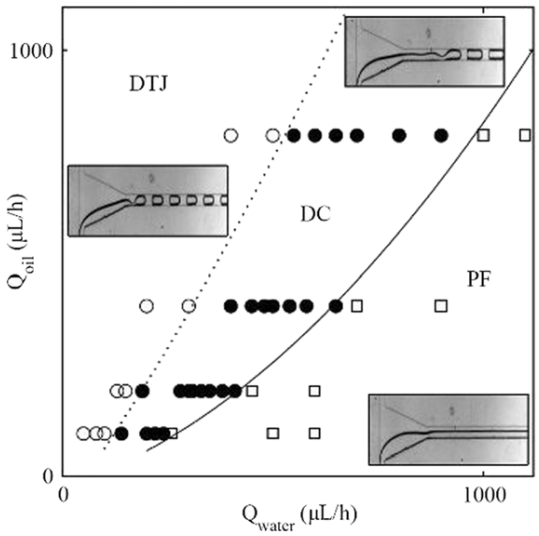

Figure 4. Droplet breakup modes for confined plug formation in microfluidic T-junctions. As the dispersed phase flow rate increases, direct breakup near the junction gives way to an extended thread that breaks downstream. For even larger flow rates, the two streams co-flow parallel to one another. (Reprinted with permission from [62], Copyright 2005, by the American Physical Society.)

3.2.3. Influence of viscosity ratio. It is notable that the viscosity ratio λ does not appear in any of the simple models given in Equations (7)–(17), except for the minor correction factor C_λ used in equation (10). Experimental studies investigating the influence of viscosity have primarily focused on changing the continuous phase viscosity, focusing on either the extremes of confined or unconfined breakup. For a given set of flow rates, increasing the viscosity of the continuous phase liquid results in decreased droplet size in unconfined conditions [27, 40]. This result is easily understood by recognizing that a larger continuous phase viscosity results in larger local shear stresses exerted at the interface, thus facilitating droplet breakup. This effect is captured in the definition of the capillary number, as Husny and co-workers demonstrated by showing that the measured droplet size falls on a single master curve when plotted as a function of the capillary number, for several different values of the viscosity ratio. Similarly, in confined breakup of plugs, the droplet length is found to be independent of the continuous phase viscosity over a wide range of oil viscosities [59], consistent with the prediction that the droplet size is dependent only on the flow rate ratio (cf equation (15)). On the other hand, the numerical study of de Menech *et al* demonstrates that the viscosity ratio is indeed important to the droplet formation process in the intermediate regime where both shear stress and confinement strongly influence the shape of the emerging droplet [56]. As the authors point out, a simple model describing these effects is difficult to obtain; however, similar effects have also been observed experimentally [51]. In addition, the dispersed phase viscosity appears to influence the critical capillary number at the transition from plug formation to stable, parallel flowing streams [61, 62]. Experiments show that the critical capillary number decreases as the viscosity ratio increases, presumably since a larger internal viscosity enhances the stability of the interface.

The formation of gas bubbles in the surrounding liquid corresponds to very low viscosity ratios. Several studies have examined bubble formation in both confined and unconfined cross-flowing streams [59, 63]. In both cases, the same general trends are observed as for breakup of liquid droplets, where the capillary number is the controlling factor in the breakup of unconfined bubbles [63] and the flow rate ratio is the controlling factor in confined systems [59]. The lengths of small bubbles produced in confined pinchoff are predicted by equation (15). As flow rate increases, measured bubble lengths are larger than predicted. The authors argue that the flow resistance in the obstructed channel is smaller in the presence of gas bubbles as compared with liquid droplets, resulting in a smaller squeezing pressure. Smaller squeezing pressure leads to a longer detachment time, allowing more influx of the dispersed gas prior to detachment and subsequently larger bubbles [59].

3.3. Focusing a jet via elongational stresses

As an alternative to the two methods described above, in which droplets are formed within predominantly shearing flows, elongational flows can efficiently form jets and small droplets. Several techniques have been developed recently that take advantage of elongational flows. Two notable examples at the macroscale are capillary flow focusing [17, 18] and selective withdrawal [16]. In selective withdrawal, an initially flat liquid interface is deformed into a cusp and then withdrawn through a capillary via an applied suction flow. In one version of capillary flow focusing, gas is forced out of a capillary into a bath of liquid. The capillary is positioned above an orifice in a large plate, and the pressure-driven contraction flow of the external liquid through the orifice focuses the gas into a thin jet. The jet subsequently breaks into equal-sized bubbles. Similar experiments have been performed using gas–liquid, liquid–gas and liquid–liquid pairs [17, 18]. Both capillary flow focusing and selective withdrawal produce highly monodisperse droplets with diameters below 100 μm, significantly smaller than the capillary tube. In flow focusing, the droplet or bubble size varies with the imposed flow rates or pressures.

The flow focusing approach was first implemented in a microfluidic geometry by Anna *et al* [64]. In microfluidic flow focusing, two immiscible liquids flow coaxially into separate channels in a planar geometry, with the continuous phase liquid flowing on either side of the dispersed phase liquid. Downstream, the two liquids come into contact at the tip of the inner microchannel. Just beyond this region, the liquids flow together through a contraction. The resulting elongation-dominated velocity field in the outer liquid draws the inner liquid into a thin jet that breaks into droplets. A schematic illustration of a flow focusing device is shown in figure 1(*c*). Planar microfluidic flow focusing devices have been used in conjunction with pressure-driven flows to generate monodisperse droplets [52,65–68] and bubbles [36, 37, 69, 70]. Syringe pump controlled volumetric flow rates are most commonly used to form droplets, while in bubble formation a constant pressure source is typically used to control the flow of the gas phase. Ward *et al* [71] recently reported qualitative differences in the observed droplet size when flow rate is controlled compared with that when pressure is controlled. The key observation in this work is that the droplet size varies much more strongly with changes in pressure than with changes in flow rate, even though the two parameters are linearly related to each other in a single-phase flow. The differences, while not fully explained, are attributed to the nonlinearities introduced by surface tension. In addition to planar devices, axisymmetric and three-dimensional microfluidic devices have also been fabricated, and the resulting droplet sizes and breakup regimes are qualitatively similar [41, 43, 44, 72]. Three-dimensional devices suffer from fewer problems with competitive wetting between the two liquids, and typically offer more robust construction, allowing for higher throughput.

A reasonable estimate of the capillary number *Ca* for flow focusing in planar geometries is based on the effective elongation rate $G = \Delta V/\Delta Z$, where $\Delta V = V_{\text{orifice}} - V_{\text{up}}$ is the velocity difference experienced by the continuous phase liquid as it flows into the orifice, and ΔZ is the distance from the end of the inner microchannel to the orifice entrance. The capillary number is given by

$$Ca = \frac{\mu_c G w_d}{2\sigma} = \frac{\mu_c w_d \Delta V}{2\sigma \Delta Z} = \frac{\mu_c w_d Q_c}{2\sigma h \Delta Z}\left[\frac{1}{w_{or}} - \frac{1}{2w_c}\right], \tag{18}$$

where w_{or} is the width of the orifice [52]. The dimension $w_d/2$ denotes the half-width of the upstream inner channel, which is analogous to the undeformed droplet radius in classic studies

of the dynamics of isolated droplets in linear flows. When droplet or bubble breakup experiments are performed over a wide range of flow rates in microfluidic flow focusing, several distinct flow regimes are observed. Nearly all experimental studies report some type of dripping and jetting regimes, and a few studies report the observation of other breakup regimes. Images of droplet breakup in dripping and jetting modes for a flow focusing device are shown in figures 2(*e*) and (*f*). The transitions between these regimes depend on the magnitudes of the imposed flow rates or pressures, or in dimensionless terms, the capillary number Ca and the flow rate ratio φ. Within each regime, the droplet size and frequency of breakup also varies with the flow parameters. Unlike in co-flowing and cross-flowing configurations, no simple model exists that can predict the droplet size as a function of control parameters in microfluidic flow focusing, in which capillary pressure and viscous stresses are generally significantly more important than inertia. However, several numerical studies have helped to elucidate the scaling behaviour in these regimes [28,73–75]. For the most part, proposed scaling arguments still need to be systematically validated experimentally.

The dripping regime is characterized by droplets that pinch off within one characteristic diameter of the flow focusing orifice, while the portion of the interface left behind after pinchoff remains at a fixed location within the orifice [52, 68, 72]. In this regime, the droplets are smaller than the orifice size and are highly monodisperse (polydispersity $< 2\%$). The droplet diameter decreases continuously with increasing capillary number and decreasing flow rate ratio, although quantitative comparison of measurements with scaling theory has not been systematically reported. Zhou *et al* [28] argue that the mechanism for droplet pinchoff in the dripping regime is a mixture of capillary instabilities, including the classic Rayleigh capillary instability [76, 77] and an end-pinching mechanism [78], combined with viscous drag on the emerging droplet from the outer liquid, which stretches and thins the necked region behind the droplet. This conclusion is based on the observation that the numerically predicted droplet size does not scale as expected for *either* a capillary wave instability, in which the scaling $d/w_{or} \sim \varphi^{1/2}$ holds, or for breakup due purely to viscous drag, in which the scaling $d/w_{or} \sim \sigma\varphi^{1/2}w_o^2/\mu_c Q_c \sim \sigma\varphi^{3/2}w_o^2/\mu_c Q_d$ holds. Note in particular that the scaling predicts that the droplet size depends on the width of the downstream tube, w_o, and also that the scaling with flow rate ratio will be different depending on whether the outer flow rate is held fixed, or the inner flow rate.

As the capillary number increases, a transition from dripping to jetting is observed. In jetting, the dispersed phase finger extends at least three orifice diameters beyond the exit of the orifice and resembles a long jet [72]. The jet interface exhibits undulations that grow until discrete droplets pinch off. The resulting droplets are larger than in dripping mode, and less uniform. Utada *et al* [72] and Zhou *et al* [28] each offer different arguments for the crossover conditions between dripping and jetting. Utada *et al* argue that the transition will occur when the timescale for visco-capillary pinchoff is comparable to the timescale for growth of the jet, leading to a critical capillary number for the transition given by $Ca_{cr} = t_{pinch}/t_{growth} = \mu_c Q_d/\sigma R_{jet}^2 \sim 1$. When $Ca < Ca_{cr}$, the interface instability will grow as soon as the emerging jet is long enough to sustain an instability, consistent with dripping, whereas for $Ca > Ca_{cr}$, viscous stresses on the interface are large enough to suppress the instability and allow for a longer thread. Zhou *et al* argue similarly that dripping will give way to jetting when disturbances on the interface are convected downstream before they can be amplified. This leads to a critical Weber number for the transition given by $We_{cr} \sim \rho_d R_{jet}^3 V_{jet}^2/\sigma\lambda_w^2$, where R_{jet} and V_{jet} are the radius and velocity of the jet, respectively, and λ_w is the wavelength of the capillary wave. Analysing this expression leads to the conclusion that the critical Weber number for the transition scales as $We_{cr} \sim \varphi^{-1/2}$ if the inner liquid flow rate Q_d is held fixed, or as $We_{cr} \sim \varphi^{3/2}$ if the outer liquid flow rate Q_c is held fixed. These scaling behaviors have not been compared with experiments.

Similar arguments for the dripping-jetting transition arise from more detailed stability analysis. For example, Ganan-Calvo [79,80] performed a linear stability analysis of a focused liquid thread stretching in an extensional flow. The analysis shows that the dripping-jetting transition can be described by a convective-absolute instability in which the dripping mode is characterized by an absolutely unstable jet, and the jetting mode is characterized by a convectively unstable jet, in which disturbances can be carried downstream along the jet for a distance prior to breakup [79, 80]. The authors report calculation of the critical values of We and Ca for the transition, parametrized by the density and viscosity ratios. Along the same lines, Hardt [81] analysed the stability of a focused thread in a gradually converging channel and found a similar progression of droplet breakup modes to those observed in experiments. This study predicts the location of jet breakup, showing that this location can reside within the focusing orifice or beyond it.

In jetting, the droplet size is proportional to the jet size. Utada *et al* [72] reported good agreement with experiments in an axisymmetric geometry when they assumed that the droplet volume is proportional to the product of the rate of flow into the jet and the characteristic pinch time for a viscous thread $t_{pinch} \sim R_{jet}\mu_c/\sigma$, leading to the estimate

$$d = 2\left(\frac{15Q_d}{\pi}\frac{R_{jet}\mu_c}{\sigma}\right)^{1/3}. \tag{19}$$

The formation of bubbles in flow focusing is similar to that of droplets, although a few additional breakup modes have been reported. Garstecki *et al* [65] report that for extremely small capillary numbers, $10^{-1} < Ca < 10^{-3}$, the bubble volume is proportional to the gas pressure and inversely proportional to the liquid flow rate and the liquid viscosity:

$$V_b \propto p_d/\mu_c Q_c. \tag{20}$$

This relationship has been confirmed numerically [38, 74] and in separate experiments [69]. The authors rationalize this observation by suggesting that the pinchoff of a bubble in this regime is driven solely by the increased pressure arising from the obstruction of the orifice by the emerging finger. The argument is similar to that used above for the formation of plugs in confined cross-flowing streams [59]. The mechanism works as follows: initially, the dispersed phase liquid is drawn into the orifice, forcing the continuous phase liquid to flow in a narrow

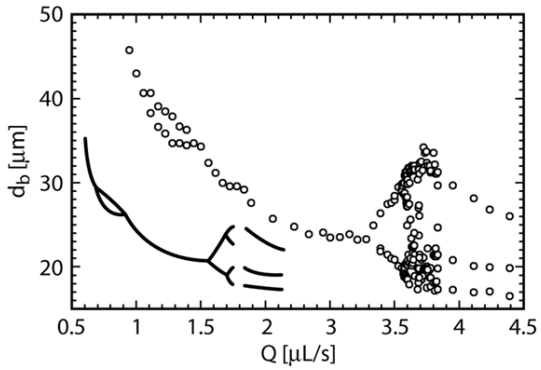

Figure 5. Nonlinear behaviour of an 'inverted dripping faucet' observed in bubble formation in microfluidic flow focusing. Period doubling, tripling and halving bifurcations in the bubble diameter are observed as the flow rate increases. (Reprinted with permission from [37], Copyright 2005, by the American Physical Society.)

region around the interface. To maintain the applied flow rate, a higher pressure is needed in the continuous liquid stream in order to drive flow through the narrow region. The higher upstream pressure leads to pinching of the interface, which progresses until a discrete bubble separates from the initial finger. Once the bubble has formed, the gas finger retracts to a position upstream of the orifice. In this same regime, the authors note the observation that the collapse rate of the bubble neck is proportional to the liquid flow rate, but is independent of the surface tension and the liquid viscosity. Furthermore, the authors argue that the lack of dependence on capillary pressure suggests that the liquid interface is stable against capillary wave instabilities throughout most of the pinchoff process. Indeed, a comparison of digitized interfaces with computed equilibrium shapes shows excellent agreement throughout the process. The observed capillary-independent scaling was also observed in numerical simulations in planar geometries [28], but numerical simulations in axisymmetric geometries show the expected dependence of collapse velocity on surface tension [38, 74]. A recent, more general stability analysis of the bubble collapse in rectangular contractions with varying aspect ratio shows that indeed, the squeezing of the bubble thread occurs due to the liquid flow around the thread until the minimum width of the thread falls below the height of the channel. At this point, radial squeezing begins and the final rapid collapse of the bubble occurs due to the inertia of the two fluids rather than a capillary instability [35]. The aspect ratio in fact controls the rate of pinching, such that more reproducible bubble formation is possible when the aspect ratio w_{or}/h is larger. While the axisymmetric simulations [74] suggest that the bubble volume scales with the downstream tube diameter, as $V_b \propto d_o^4$, this scaling has not been validated experimentally. A similar pinchoff behaviour has also been reported in droplet formation [52], but the above scaling behaviour has not been quantified for those experiments. Finally, bubble pinchoff exhibits a rich dynamical behaviour at moderate values of the Weber number [37]. As figure 5 shows, period doubling bifurcations and apparently chaotic behaviour have been observed, consistent with the well-known behaviour of dripping faucets at the macroscale [11].

In addition to the droplet size and the critical parameters between transitions, parameters such as the droplet formation frequency f, the droplet spacing s, and the droplet velocity U have also been measured. Specifically, Ward *et al* [71] suggest that geometric arguments lead to the relationship

$$fs = U, \tag{21}$$

and found that this relationship holds experimentally, when independent measurements of all three variables are compared.

3.3.1. Generating sub-micron droplets in microfluidics. Despite the promise of microfluidic droplet technologies, the droplet sizes produced in all of the above geometries are rarely smaller than a few micrometres in diameter, largely because the pinchoff process is strongly influenced by the smallest feature size in the device (i.e. the constriction orifice or junction geometry) [64, 65]. Microfluidic methods for producing droplets smaller than one-tenth of the orifice size are relatively few. For example, electrohydrodynamic jetting has been implemented in a microfluidic device to produce particles 1–10 μm in size [11]. The resulting particles are highly polydisperse compared with other microfluidic droplet formation methods. Tan and Lee [67, 82, 83] observed the formation of tiny satellite droplets in between the primary droplets, and developed a microfluidic separator to collect these satellites. Most recently, Anna and Mayer [52] reported on a new mode of droplet formation that occurs in the presence of dissolved surfactants. At surfactant concentrations near the critical micelle concentration (CMC), and in a specific range of Ca and φ values, the authors observe that the emerging droplet forms a conical shape, and that tiny liquid threads stream from the tip of the cone. Images from these experiments are shown in figure 6(*a*). The liquid threads grow longer as the flow rate ratio decreases, and subsequently break into a series of tiny droplets, one or two microns in diameter. The observed process resembles a phenomenon called 'tipstreaming' that has previously been reported in larger scale isolated droplets in unbounded linear flows [54, 84]. Although this process appears to require surfactants to occur, two separate numerical studies report a similar tipstreaming process in flow focusing [28], and co-flowing [75] geometries, where surfactants are absent in both cases. Suryo and Basaran demonstrate that this process occurs due to the presence of a nonlinear extensional flow near the tip of the forming droplet, an observation that has previously been reported in theoretical and numerical studies [85–87]. As the outer liquid passes the tip of the inner capillary tube, the velocity field acquires a radially inward component, which must gradually convert to a purely axial velocity. This spatial dependence of the velocity field leads to a nonlinear extensional strain, which is capable of focusing the emerging finger at higher flow speeds. The authors argue that the transition to tipstreaming occurs when

$$Ca_d^{-1} < (\lambda\varphi)^{-1}, \tag{22}$$

where in this case the capillary number is defined in terms of the dispersed phase flow rate, $Ca_d = 4\mu_d Q_d/\sigma\pi w_d^2$. Images of interface shapes resulting from the numerical simulations during thread formation and tipstreaming are shown in figure 6(*b*). While experimental observations of surfactant-free tipstreaming have not been reported, it is

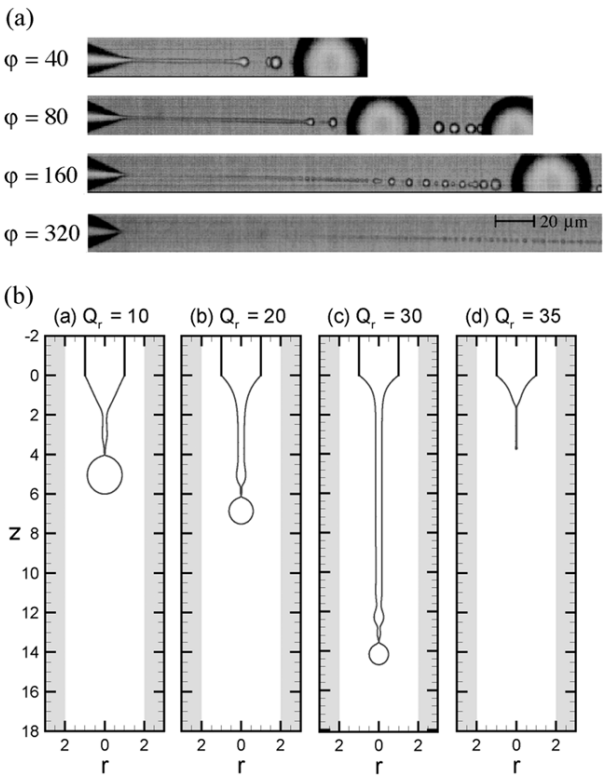

Figure 6. Images depicting tipstreaming in (*a*) flow focusing experiments using near-CMC surfactant solutions. (Reprinted with permission from [52], Copyright 2006, American Institute of Physics.) (*b*) Numerical simulations of droplet breakup in co-flowing streams. (Reprinted with permission from [75], Copyright 2006, American Institute of Physics.) In both cases, the thread length grows as the flow rate ratio φ decreases, and the critical flow rate ratio for observing tipstreaming is similar.

notable that these regimes occur at very similar values of the flow rate ratio in both experiments [52] and simulations [75].

In the microscale tipstreaming process of Anna and Mayer [52], a large droplet is formed initially, similar to the process used by Tan and Lee [83]. Thus, separation of the larger droplets will be essential to the success of any application that utilizes these micrometre-scale droplets. The size and polydispersity of the resulting micrometre-scale droplets depends on the ability of the fine liquid thread to stretch rapidly before it disintegrates. Anna and Mayer observed that the thread length increases with decreasing flow rate ratio, i.e. when the outer liquid is flowing significantly faster than the inner liquid. In addition, the thread length is observed to follow the outer flow field affinely for a time, suggesting that control over the downstream velocity profile will be a key factor in controlling the size of the resulting droplets. Finally, it is worth noting that, as droplets produced become ever smaller, the available techniques for measuring these droplets are few. Optical methods such as light microscopy have reached the limit of their resolution, while other characterization methods such as scattering techniques require large sample volumes and extended measurement timescales in order to achieve meaningful signals. Development of useful characterization techniques for microfluidics will be an important area of future research.

4. Microfluidic methods using actuation or external forces

This review is primarily focused on passive droplet breakup methods in which viscous stresses and interfacial tension lead to interfacial instabilities and the pinchoff of discrete droplets. A number of methods have also been demonstrated in which an external force is applied to actuate pinchoff. External forces offer additional handles for control over the droplet size and pinchoff frequency. We briefly review some examples of actuated microfluidic droplet breakup systems in this section.

A typical actuation mechanism utilizes a flexible membrane that is deflected using a piezoelectric transducer. A well-known example is that of 'drop on demand' inkjet printing technology, in which a droplet is forced out of a microfabricated nozzle by the deflection of a membrane in contact with the reservoir. The nozzle size is small enough that droplets are not formed unless the membrane is deflected. Similar to passive methods described above, a number of regimes exist characterizing the behaviour of droplet breakup. Specifically, droplets are not formed until the actuation voltage of the piezoactuator is increased above a critical value, at which point droplets are formed in a jetting regime [88]. The primary droplet size is a function of both fluid properties and nozzle diameter, but the actuation voltage magnitude only affects primary droplet velocity, not primary droplet size [15]. The voltage waveform used for actuation controls the formation of satellite droplets and can eliminate them entirely, leading to the reproducible formation of uniform primary droplets [14, 15].

A deflecting membrane has been used in conjunction with a microfluidic T-junction, where the membrane is positioned between the dispersed phase channel and a secondary actuation channel [89]. The actuation channel is filled with water and actuated by increasing the water pressure to deflect the membrane. Deflecting the membrane alters the instantaneous flow velocity of the dispersed phase liquid, modulating the natural frequency at which droplet production occurs. If the forcing frequency is a multiple of the natural frequency, droplet formation is periodic and occurs at a rate faster than the natural frequency of droplet production. In this case, the droplet size is observed to decrease linearly with increasing forcing frequency over a wide range of forcing frequencies. When the driving frequency is not commensurate with the natural frequency, droplet formation is irregular.

Actuated breakup has been implemented in a microfluidic flow focusing device, in which pressure chambers are placed on either side of the flow focusing orifice [90, 91]. When the chambers are actuated pneumatically, the channel walls collapse around the thread, causing it to pinch off. The resulting droplet size is a strong function of actuation frequency and the flow rate ratio used to create the fluid thread. This method has been implemented with a single actuation point [91] or with a line of 'choppers' simultaneously actuating at multiple points along the channel [90].

Electric fields offer an alternative means of actuating breakup of a liquid thread. For example, a flat interface between immiscible dielectric liquids deflects in a local electric field created by deposited electrodes [92, 93]. The deflection triggers an interfacial instability that grows, and the thread ruptures when the interface collides with the opposing wall.

In this case, the droplet size is dependent on the flow rates and the strength of the electric field. Electric fields have also been used to draw a liquid interface into a contraction [94, 95]. When this occurs, a thin jet forms and emits a droplet when it grows long enough to sustain an interfacial instability. By pulsing the electric field, this method is analogous to the 'drop on demand' inkjet printing method.

It is also possible to actuate droplet breakup by modulating the driving flow itself, through precise control of the time-dependent volumetric flow rate. In one example, flow is driven into a quiescent chamber at a desired flow rate for a specified duration. Reversing the flow at a much larger flow rate precipitates detachment by causing a sudden backpressure and necking of the thread [96]. The product of the inlet flow rate and the duration of influx of liquid determine the droplet volume. This method can successfully generate femtolitre sized droplets, a single droplet at a time, in an otherwise quiescent reservoir, but the method requires precise, programmable syringe pumps and the capability to visualize the interface as it approaches the reservoir inlet.

Finally, a few methods are inherently passive, but employ additional effects that modulate the breakup of the liquid thread. For example, if the flow of the immiscible liquids into a T-shaped microchannel is reversed from the typical configuration, such that the continuous phase liquid travels into the perpendicular side arm, a finger of the dispersed phase liquid will extend into the junction, and the squeezing flow of the continuous phase liquid will promote droplet breakup [97, 98]. As expected, the droplet breakup regimes depend on the flow rates of the continuous and dispersed phase liquids. Creating heterogeneous wetting 'patches' within a microfluidic geometry can also direct the motion of the interface and promote breakup [99]. Also, the downstream channel geometry can be used to modulate breakup. For example, expansions and contractions create pinching points that promote breakup of a liquid thread at specific locations [100]. In this case, a thread of dispersed phase liquid is generated in the usual way, but the thread does not break immediately due to viscous stabilization of the interface by flow. When the flow is stopped, the pinching points lead to the formation of an individual droplet in each expansion region. The droplet size in this case is weakly related to the dispersed phase flow rate, and strongly dependent on the chamber and channel dimensions.

5. Applications of droplets in microchannels

In this review, we have focused primarily on describing the state-of-the-art in our understanding of the mechanisms for droplet and bubble formation in microfluidic geometries. Despite the many fundamental questions that remain to be answered in this regard, it is clear that microfluidic technologies offer an efficient means of producing highly uniform droplets and bubbles, and also a convenient mechanism for manipulating their downstream motion. These capabilities have led to the development of several novel applications that could not have been realized using other technologies. We highlight a few key examples; many of them have developed a large literature of their own and some have been reviewed elsewhere. Applications of droplet-based

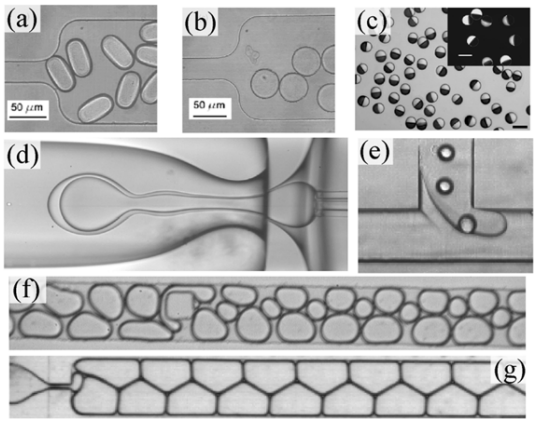

Figure 7. Examples of complex polymer particles fabricated using microfluidic droplets as templates. Nonspherical particles such as (*a*) plugs and (*b*) discs are fabricated using microchannels to confine the droplets. (Reprinted with permission from [145], Copyright 2005, American Chemical Society.) (*c*) Janus particles with two distinct halves are fabricated exploiting laminar microfluidic streams. (Reprinted with permission from [126], Copyright 2006, American Chemical Society.) Compound droplets can be created in both (*d*) flow focusing. (Reprinted from [72] with permission from AAAS) and (*e*) by applying sequential breakup in a T-junction. (Reproduced from [152] by permission of The Royal Society of Chemistry). (*f*) Asymmetric splitting can be used to create a bidisperse emulsion. (Reprinted with permission from [153], Copyright 2004 by the American Physical Society.) (*g*) Highly ordered foams can be generated using flow focusing devices. (Reprinted with permission from [154], Copyright 2006 by the American Physical Society.)

technologies fall into two major categories: (a) design of lab-on-a-chip devices using droplets as tiny reactors, and (b) synthesis of precise materials such as highly uniform micro- and nanoparticles, compound droplets, foams and emulsions.

The use of droplets as reactors for miniaturized chemical and biological assays has been extensively reviewed in a recent paper by Song *et al* [21]. The key advantage of using droplets for these reactions is that the compartmentalization of material into the droplets allows for rapid mixing, reaction and transport of tiny (femtolitre to microliter) volumes of reagents, detection and control of reaction kinetics, and manipulation of droplet contents via control over the flow streams. Droplet-based assays have already been demonstrated for protein crystallization [101], enzyme kinetics studies [102], DNA and blood analysis [103–105] and others [2]. Droplets formed in microfluidic processes have also been used as reactors for synthesizing uniform nanoparticles [106–108]. In the design of droplet-based devices, the key challenges include controlling and accelerating mixing inside droplets [109, 110], preventing or promoting coalescence of droplets [111–113], sorting and directing droplet motion based on the information they contain [114–116], and detecting the results of compartmentalized reactions [117, 118]. Droplets are also convenient vessels for encapsulation, protection and transport of cells, and the development of cell-based assays [119–122].

Highly uniform droplets facilitate the synthesis of a wide variety of useful and novel materials. Several examples are shown in figure 7. For example, synthesis of solid microparticles simply requires a method of solidifying the droplet interior. Droplets can be created using co-flowing

Table 1. Summary of solid microparticles fabricated using microfluidic droplet formation methods to template the synthesis. The particle composition and solidification procedure are listed.

Geometry	Solidification process	Particle composition
Flow Focusing	Self assembly	• Polystyrene–polymethylmethacrylate block copolymer [123]
	UV photo-polymerization *ex situ*	• Dextran-hydroxyethyl methacrylate hydrogel [124]
	UV photo-polymerization *in situ*	• Polymethacrylate [125] • Methacryloxypropyl dimethylsiloxane [126] • Poly(ethylene glycol) diacrylate with pentaerythritol triacrylate [126] • Tripropyleneglycol diacrylate [127–130] • Ethyleneglycol diacrylate [131] • Divinylbenzene [131] • Ethyleneglycol dimethacrylate [127, 132] • Pentaerythritol triacrylate [131, 132] • Pentaerythritol tetraacrylate [128, 132] • Acrylamide [133] • Dimethacrylate oxypropyldimethylsiloxane [128]
	Solvent extraction	• Polystyrene [134] • Polystyrene, alginate, poly(lactic-co-glycolic acid) [135]
	Ionic crosslinking	• Calcium alginate [136–139] • Chitosan [140]
	Cooling of molten material	• Polystyrene [134] • Gelucire [134] • Agarose [128]
Cross-flowing streams	Self assembly	• Organosilane [141]
	Thermal polymerization *ex situ*	• Polydivinylbenzene [142] • Polystyrene [143] • 1,6 Hexanediol diacrylate [57] • Isobornyl acrylate [57, 144]
	UV photo-polymerization *in situ*	• Norland Optical Adhesive 60 [145]
	UV photo-polymerization *ex situ*	• Polymethylacrylic acid with Ethyleneglycol dimethacrylate [146] • 1,6 Hexanediol diacrylate [57] • Isobornyl acrylate [57]
Co-flowing streams	UV photo-polymerization *in situ*	• 4-Hydroxybuthyl acrylate [147]
	Solvent extraction	• Mixed metal oxide hollow spheres [131]
	Redox-initiated crosslinking	• N-isopropylacrylamide [129]

streams, cross-flowing streams or flow focusing geometries, as long as the dispersed phase liquid consists of a primer material that can be solidified or hardened through initiation downstream. Most processes to date make use of polymers that are crosslinked either through thermal initiation or photo-polymerization, while metallic particles and biopolymers have been synthesized via self-assembly and biochemical crosslinking. Table 1 summarizes the main processes and materials that have been used to make microparticles, where microfluidic droplet breakup has specifically been used to create the template for the particle. We distinguish between solidification processes that occur *in situ* within a microfluidic device, and those in which droplets are fabricated in a microfluidic device and then solidified in a batch reactor outside of the microdevice. The table demonstrates that a wide variety of materials and solidification processes are feasible for microparticle fabrication within microchannels.

In addition to homogeneous particles the flexibility of microfluidics also allows the design of compact processes to fabricate more complex particles. Some examples, with a selection of representative images shown in figure 7, include Janus particles, which contain two distinct parts with different wetting properties [126, 133, 144], particles with embedded colloids or nanoparticles [134, 143], core-shell particles [123, 127, 131] and particles imprinted with specific molecules [146]. Non-spherical particles have been fabricated by adjusting channel dimensions downstream [133, 145]. Spherical capsules have been fabricated by polymerizing the interface of microfluidic droplets [130], and cylindrical capsules have been fabricated via a combination of hydrodynamic focusing of a viscoelastic jet and stabilization of the interface with particles [148]. For a more comprehensive look at microparticle fabrication we suggest a number of recent reviews [141,149–151].

One of the more interesting examples of a complex particle is a compound droplet or 'double emulsion', consisting of a collection of droplets within another droplet, which is itself surrounded by an external liquid. Such constructions are valuable in particular for applications in which controlled delivery of a drug or other species is desired; however, fabrication is difficult to control in conventional processes. Microfluidic droplet formation has proved useful for fabrication of compound droplets, in which the size, number and composition of both the internal and external droplets can be tuned. Controlling the wettability of the microchannel walls is one key to successful formation of compound droplets [43, 155]. Compound droplets have been

formed via sequential application of microfluidic droplet breakup in T-shaped cross-flow junctions (see figure 7(*e*)) [152,156], and via coaxial co-flowing streams in axisymmetric flow focusing devices (see figure 7(*d*)) [43,72]. Utada *et al* [72] provide simple scaling arguments to show how the internal and external droplet sizes depend on the applied flow rates. Zhou *et al* reproduce this process numerically, and demonstrate through simulations that the successful encapsulation of a droplet inside another droplet occurs when the capillary wave instabilities along each of the liquid–liquid interfaces are coordinated. Furthermore, the breakup of the inner jet is purely capillary wave driven, while the outer interface breaks up due to a combination of viscous drag on the interface and capillary wave instabilities. The difficulty in coordinating these two processes leads to the observation in both experiments and numerics that compound droplet formation is more irregular than the formation of simple droplets in microfluidic processes. In principle, the number of droplets encapsulated is related to the ratio of the most unstable wavelengths, which is in turn related to the ratio of applied flow rates. Numerical simulations have only achieved encapsulation of up to two droplets [28], while several droplets have been successfully encapsulated experimentally [72] using these principles.

Collections of monodisperse particles form highly ordered arrays; modifying the particle shapes or introducing additional controlled size populations allows for even more interesting self-assembled structures (see figure 7(*f*)) [157]. Ordered arrays of microdroplets have been used as an alternative to standard well-plates for protein crystallization assays [158]. More fundamentally, ordered arrays of droplets exhibit surprising long-range interactions that lead to collective normal vibration modes, analogous to phonons [159]. Numerous studies have focused on the production of foams; fabrication of devices in glass rather than polymers allows high rate production of uniform foams [47]. The flow behaviour and structure of these foams has been examined in detail when confined within microfluidic channels (see figure 7(*g*)) [154,160–162]. Garstecki and co-workers [163] have recently demonstrated that ordered foams can be used as stable diffraction gratings in which the pitch, or diffraction angle, can be tuned by varying the flow rates and pressures applied to the system.

6. Summary

Microfluidics has emerged as a versatile approach to generating continuous streams of uniform emulsion droplets. Several related microfluidic methods have developed based on pressure-driven flow of immiscible liquids in a complex microfluidic junction. We have organized these methods into three categories based on the flow field in the junction: methods that utilize co-flowing fluid streams to break droplets, methods that utilize cross-flowing fluid streams and methods that utilize elongational flows. Each of these methods produces droplets comparable in size to the characteristic geometric length scales of the device, in a steady, periodic manner. Droplet sizes depend on the volumetric flow rate or pressure imposed in each liquid phase to drive the flow; in general droplet sizes range from 1 to 100 μm in diameter, corresponding to volumes ranging from femtolitres to nanoliters. The droplet sizes are very uniform, with polydispersity as low as 1–3%.

Examining the mechanisms for droplet breakup in each of the three primary geometries, several common themes emerge. In all cases, droplet formation appears to occur in a nominally two-stage process. Initially, fluid stresses in the neighbourhood of the emerging droplet interface act to stretch and deform the interface. Some time later, the neck of the droplet begins to thin. During thinning, the droplet continues to fill with dispersed phase liquid. The final size of the droplet depends on the volume of liquid that was able to enter the droplet prior to breaking of the neck. The droplet diameter decreases as the capillary number increases, due to increased viscous stresses acting to deform the droplet. The droplet diameter increases as the ratio of flow rates increases, since the emerging droplet can be filled at a relatively higher rate. The precise dependence of droplet size on the flow parameters depends on the specific geometry considered.

In microfluidic droplet formation using co-flowing streams and flow focusing geometries, two predominant modes of droplet breakup are observed. At low capillary numbers, dripping is observed, in which droplets pinch off near the junction. As the capillary number increases, the emerging finger remains stable for a distance downstream prior to breaking. This mode is called ‘jetting’. In all cases the transitions have been characterized as well as the droplet size variation within each regime. A simple phenomenological model has been proposed to predict the resulting droplet size in the co-flowing geometry; a similar model is not available for microfluidic flow focusing. In cross-flowing streams, the breakup dynamics depend on how strongly the cross-flow junction confines the emerging droplet. When the droplet is unconfined, the capillary number controls the droplet size and small spherical droplets form. However, confinement modifies the scaling behaviour even at high capillary numbers. When the droplet is highly confined, the flow rate ratio controls the droplet size, and droplets form long slugs in the downstream channel. Simple models have been proposed for cross-flow geometries as well, although these seem to be specific to the precise geometry of the device. Finally, additional interesting droplet breakup modes have been reported, including a bubble breakup mode at very low capillary number in which pinching of the neck appears to be independent of capillary pressure. In flow focusing, surfactants dissolved in the liquids lead to the formation of very fine threads in a specific range of flow rates. This ‘tipstreaming’ phenomenon may be useful for the production of very tiny droplets.

Numerous novel applications have emerged based on these capabilities, ranging from the synthesis of precise emulsions, foams and particles, to the design of miniaturized biochemical assays. Despite the progress in these areas to date, there are still many possibilities for future research and development. Fundamentally, there are still numerous questions that remain about the mechanisms for droplet breakup. Particularly in the flow focusing geometry, there is not a simple mechanistic model available that can predict droplet size over a wide range of flow conditions. On the other hand, scaling behaviour has been suggested but experimental validation of the suggested scaling is not available for most cases. In cross-flowing streams, the crossover from unconfined to confined breakup,

in which both viscous stresses and pinching pressure due to obstruction of the channel are likely to be important, has not been well characterized. Finally, the recent observation that pressure control yields different scaling of the droplet size than volumetric flow rate control has not been explained.

In addition to the basic droplet formation mechanisms, several possibilities have emerged for further control over the droplet formation process. Obtaining a deeper understanding of the mechanisms underlying the tipstreaming process will allow greater control over the sustained formation of fine-scale droplets. Developments in this area would need to be accompanied by development of *in situ* characterization methods for detecting and measuring fine-scale droplets as they form. Viscoelastic behaviour in the dispersed phase will also strongly influence droplet breakup and can potentially be exploited to generate stable filaments. Finally, scaling of these processes to increase yield and throughput will necessitate engineering of interconnected microchannels, and an understanding of the dynamical behaviour of interacting elements within these networks. As new capabilities emerge, the possibility for development of new applications of droplet-based microfluidic systems will continue to grow.

Acknowledgments

The authors thank the National Science Foundation (CBET-0608864) and the Pennsylvania Infrastructure Technology Alliance for financial support during the writing of this review. In addition, they are grateful to Howard Stone, Piotr Garstecki, Pierre Guillot and Jan-Paul Raven for insightful comments and helpful additions to this review.

References

[1] Schramm L L 2005 *Emulsions, Foams, and Suspensions: Fundamentals and Applications* (New York: Wiley)
[2] Griffiths A D and Tawfik D S 2006 *Trends in Biotechnology* **24** 395–402
[3] Squires T M and Quake S R 2005 *Rev. Mod. Phys.* **77** 977–1026
[4] Stone H A, Stroock A D and Ajdari A 2004 *Ann. Rev. Fluid Mech.* **36** 381–411
[5] Joscelyne S M and Tragardh G 2000 *J. Membr. Sci.* **169** 107–17
[6] Kobayashi I and Nakajima M 2006 *J. Japan. Soc. Food Sci. Technol.-Nippon Shokuhin Kagaku Kogaku Kaishi* **53** 317–26
[7] Tong J H, Nakajima M and Nabetani H 2002 *Eur. J. Lipid Sci. Technol.* **104** 216–21
[8] Haverkamp V, Hessel V, Lowe H, Menges G, Warnier M J F, Rebrov E V, de Croon M, Schouten J C and Liauw M A 2006 *Chem. Eng. Technol.* **29** 1015–26
[9] Losey M W, Schmidt M A and Jensen K F 2001 *Ind. Eng. Chem. Res.* **40** 2555–62
[10] Sugiura S, Nakajima M, Iwamoto S and Seki M 2001 *Langmuir* **17** 5562–6
[11] Basaran O A 2002 *AIChE J.* **48** 1842–8
[12] Villermaux E 2007 *Annu. Rev. Fluid Mech.* **39** 419–46
[13] Chen A U and Basaran O A 2002 *Phys. Fluids* **14** L1–L4
[14] Dong H M, Carr W W and Morris J F 2006 *Rev. Sci. Instrum.* **77** 085101
[15] Dong H M, Carr W W and Morris J F 2006 *Phys. Fluids* **18** 072102
[16] Cohen I, Brenner M P, Eggers J and Nagel S R 1999 *Phys. Rev. Lett.* **83** 1147–50
[17] Ganan-Calvo A M 2004 *Phys. Rev.* E **69** 027301
[18] Gañán-Calvo A M 1998 *Phys. Rev. Lett.* **80** 285–8
[19] Umbanhowar P B, Prasad V and Weitz D A 2000 *Langmuir* **16** 347–51
[20] Song H, Tice J D and Ismagilov R F 2003 *Angew. Chem. Int. Edn* **42** 768–72
[21] Song H, Chen D L and Ismagilov R F 2006 *Angew. Chem. Int. Edn* **45** 7336–56
[22] Jensen K and Lee A 2004 *Lab Chip* **4** 31N–2N
[23] Atencia J and Beebe D J 2005 *Nature* **437** 648–55
[24] Baroud C N and Willaime H 2004 *C. R. Phys.* **5** 547–55
[25] Gunther A and Jensen K F 2006 *Lab Chip* **6** 1487–503
[26] Cho S K, Fan S-K, Moon H and Kim C-J 2002 *IEEE Trans.* 32–5
[27] Husny J and Cooper-White J J 2006 *J. Non-Newton. Fluid Mech.* **137** 121-36
[28] Zhou C F, Yue P T and Feng J J 2006 *Phys. Fluids* **18** 092105
[29] Duffy D C, McDonald J C, Schueller O J A and Whitesides G M 1998 *Anal. Chem.* **70** 4974–84
[30] Husny J, Jin H Y, Harvey E C and Cooper-White J 2006 *Smart Mater. Struct.* **15** S117–23
[31] Madou M J 1998 *Fundamentals of Microfabrication* (Boca Raton, FL: CRC Press)
[32] Stone H A 2005 *Chem. Eng. Sci.* **60** 4838–45
[33] Stone H A 1994 *Ann. Rev. Fluid Mech.* **26** 65–102
[34] Bentley B J and Leal L G 1986 *J. Fluid Mech.* **167** 219–40
[35] Dollet B, van Hoeve W, Raven J P, Marmottant P, Versluis M 2007 *Phys. Rev.* E submitted
[36] Garstecki P, Gitlin I, DiLuzio W, Whitesides G M, Kumacheva E and Stone H A 2004 *Appl. Phys. Lett.* **85** 2649–51
[37] Garstecki P, Fuerstman M J and Whitesides G M 2005 *Phys. Rev. Lett.* **94** 234502
[38] Weber M W and Shandas R 2007 *Microfluid. Nanofluid.* **3** 195–206
[39] Dreyfus R, Tabeling P and Willaime H 2003 *Phys. Rev. Lett.* **90** 144505
[40] Xu J H, Li S W, Tan J, Wang Y J and Luo G S 2006 *AIChE J.* **52** 3005-10
[41] Yobas L, Martens S, Ong W L and Ranganathan N 2006 *Lab Chip* **6** 1073–9
[42] Xu J H, Li S W, Tan J, Wang Y J and Luo G S 2006 *Langmuir* **22** 7943–6
[43] Huang S H, Tan W H, Tseng F G and Takeuchi S 2006 *J. Micromech. Microeng.* **16** 2336–44
[44] Takeuchi S, Garstecki P, Weibel D B and Whitesides G M 2005 *Adv. Mater.* **17** 1067
[45] Cubaud T, Ulmanella U and Ho C M 2006 *Fluid Dyn. Res.* **38** 772–86
[46] Cygan Z T, Cabral J T, Beers K L and Amis E J 2005 *Langmuir* **21** 3629–34
[47] Lorenceau E, Sang Y Y C, Hohler R and Cohen-Addad S 2006 *Phys. Fluids* **18** 097103
[48] Cramer C, Fischer P and Windhab E J 2004 *Chem. Eng. Sci.* **59** 3045–58
[49] Zhang D F and Stone H A 1997 *Phys. Fluids* **9** 2234–42
[50] Guillot P, Colin A, Utada A S and Ajdari A 2007 *Phys. Rev. Lett.* submitted
[51] Anna S L, Christopher G F and Noharuddin N 2005 *ASME Int. Mech. Eng. Congress* (*Orlando, FL*) 80625
[52] Anna S L and Mayer H C 2006 *Phys. Fluids* **18** 121512
[53] Thorsen T, Roberts R W, Arnold F H and Quake S R 2001 *Phys. Rev. Lett.* **86** 4163–6
[54] Taylor G I 1934 *Proc. R. Soc.* A **146** 501–23
[55] Barbier V, Willaime H, Tabeling P and Jousse F 2006 *Phys. Rev.* E **74** 046306
[56] de Menech M, Garstecki P, Jousse F and Stone H A 2007 *J. Fluid Mech.* under review
[57] Nisisako T, Torii T and Higuchi T 2004 *Chem. Eng. J.* **101** 23–9

[58] Xu J H, Luo G S, Chen G G and Wang J D 2005 *J. Membr. Sci.* **266** 121–31
[59] Garstecki P, Fuerstman M J, Stone H A and Whitesides G M 2006 *Lab Chip* **6** 437–46
[60] van der Graaf S, Nisisako T, Schroen C, van der Sman R G M and Boom R M 2006 *Langmuir* **22** 4144–52
[61] Tice J D, Lyon A D and Ismagilov R F 2004 *Anal. Chim. Acta* **507** 73–7
[62] Guillot P and Colin A 2005 *Phys. Rev.* E **72** 066301
[63] Xu J H, Li S, Chen G G and Luo G S 2006 *AIChE J.* **52** 2254–9
[64] Anna S L, Bontoux N and Stone H A 2003 *Appl. Phys. Lett.* **82** 364–6
[65] Garstecki P, Stone H A and Whitesides G M 2005 *Phys. Rev. Lett.* **94** 164501
[66] Haeberle S, Zengerle R and Ducree J 2007 *Microfluid. Nanofluid.* **3** 65–75
[67] Tan Y C, Fisher J S, Lee A I, Cristini V and Lee A P 2004 *Lab Chip* **4** 292–8
[68] Xu Q Y and Nakajima M 2004 *Appl. Phys. Lett.* **85** 3726–8
[69] Cubaud T, Tatineni M, Zhong X L and Ho C M 2005 *Phys. Rev.* E **72** 037302
[70] Garstecki P, Fuerstman M J and Whitesides G M 2005 *Nature Phys.* **1** 168–71
[71] Ward T, Faivre M, Abkarian M and Stone H A 2005 *Electrophoresis* **26** 3716–24
[72] Utada A S, Lorenceau E, Link D R, Kaplan P D, Stone H A and Weitz D A 2005 *Science* **308** 537–41
[73] Harvie D J E, Davidson M R, Cooper-White J J and Rudman M 2006 *Chem. Eng. Sci.* **61** 5149–58
[74] Jensen M J, Stone H A and Bruus H 2006 *Phys. Fluids* **18** 077103
[75] Suryo R and Basaran O A 2006 *Phys. Fluids* **18** 082102
[76] Rayleigh L 1879 *Proc. R. Soc. Lond.* **29** 71–97
[77] Tomotika S 1935 *Proc. R. Soc. A* **150** 322-37
[78] Stone H A and Leal L G 1989 *J. Fluid Mech.* **198** 399–427
[79] Ganan-Calvo A M, Herrada M A and Garstecki P 2006 *Phys. Rev. Lett.* **96** 124504
[80] Ganan-Calvo A M and Riesco-Chueca P 2006 *J. Fluid Mech.* **553** 75–84
[81] Hardt S 2005 *Phys. Fluids* **17** 100601
[82] Tan Y C, Cristini V and Lee A P 2006 *Sensors Actuators B: Chemical* **114** 350–6
[83] Tan Y C and Lee A P 2005 *Lab Chip* **5** 1178–83
[84] de Bruijn R A 1993 *Chem. Eng. Sci.* **48** 277
[85] Booty M R and Siegel M 2005 *J. Fluid Mech.* **544** 243–75
[86] Pozrikidis C 1997 *J. Fluid Mech.* **331** 145–67
[87] Sherwood J D 1984 *J. Fluid Mech.* **144** 281–95
[88] Beulen B, de Jong J, Reinten H, van den Berg M, Wijshoff H and van Dongen R 2007 *Exp. Fluids* **42** 217–24
[89] Willaime H, Barbier V, Kloul L, Maine S and Tabeling P 2006 *Phys. Rev. Lett.* **96** 054501
[90] Chen C T and Lee G B 2006 *J. Microelectromech. Syst.* **15** 1492–8
[91] Hsiung S K, Chen C T and Lee G B 2006 *J. Micromech. Microeng.* **16** 2403–10
[92] Ozen O, Aubry N, Papageorgiou D T, Petropoulos P G 2006 *Electrochim. Acta* **51** 5316–23
[93] Ozen O, Aubry N, Papageorgiou D T and Petropoulos P G 2006 *Phys. Rev. Lett.* **96** 144501
[94] He M, Kuo J S and Chiu D T 2006 *Langmuir* **22** 6408–13
[95] He M Y, Kuo J S and Chiu D T 2005 *Appl. Phys. Lett.* **87** 031916
[96] Lorenz R M, Edgar J S, Jeffries G D M and Chiu D T 2006 *Anal. Chem.* **78** 6433–9
[97] Xu J H, Li S W, Wang Y J and Luo G S 2006 *Appl. Phys. Lett.* **88** 133506
[98] Xu J H, Luo G S, Li S W and Chen G G 2006 *Lab Chip* **6** 131–6
[99] Su Y C and Lin L W 2006 *J. Micromech. Microeng.* **16** 1884–90
[100] Wu L, Li G P, Xu W and Bachman M 2006 *Appl. Phys. Lett.* **89** 144106
[101] Zheng B, Gerdts C J and Ismagilov R F 2005 *Curr. Opin. Struct. Biol.* **15** 548–55
[102] Song H and Ismagilov R F 2003 *J. Am. Chem. Soc.* **125** 14613–9
[103] Li L, Boedicker J Q and Ismagilov R F 2007 *Anal. Chem.* **79** 2756–61
[104] Song H, Li H W, Munson M S, Van Ha T G and Ismagilov R F 2006 *Anal. Chem.* **78** 4839–49
[105] Chabert M, Dorfman K D and Viovy J L 2006 *Houille Blanche-Revue Internationale De L Eau* 51-6
[106] Chan E M, Alivisatos A P and Mathies R A 2005 *J. Am. Chem. Soc.* **127** 13854–61
[107] Hung L H, Choi K M, Tseng W Y, Tan Y C, Shea K J and Lee A P 2006 *Lab Chip* **6** 174–8
[108] Shestopalov I, Tice J D and Ismagilov R F 2004 *Lab Chip* **4** 316–21
[109] Grigoriev R O, Schatz M F and Sharma V 2006 *Lab Chip* **6** 1369–72
[110] Song H, Bringer M R, Tice J D, Gerdts C J and Ismagilov R F 2003 *Appl. Phys. Lett.* **83** 4664–6
[111] Chen D L L, Li L, Reyes S, Adamson D N and Ismagilov R F 2007 *Langmuir* **23** 2255–60
[112] Link D R, Grasland-Mongrain E, Duri A, Sarrazin F, Cheng Z D, Cristobal G, Marquez M and Weitz D A 2006 *Angew. Chem. Int. Edn* **45** 2556–60
[113] Liu K, Ding H J, Chen Y and Zhao X Z 2007 *Microfluid. Nanofluid.* **3** 239–43
[114] Cheow L F, Yobas L and Kwong D L 2007 *Appl. Phys. Lett.* **90** 054107
[115] Fuerstman M J, Garstecki P and Whitesides G M 2007 *Science* **315** 828–32
[116] Yamada M and Seki M 2006 *Anal. Chem.* **78** 1357–62
[117] Cristobal G, Arbouet L, Sarrazin F, Talaga D, Bruneel J L, Joanicot M and Servant L 2006 *Lab Chip* **6** 11406
[118] Strehle K R, Cialla D, Rosch P, Henkel T, Kohler M and Popp J 2007 *Anal. Chem.* **79** 1542–7
[119] He M Y, Edgar J S, Jeffries G D M, Lorenz R M, Shelby J P and Chiu D T 2005 *Anal. Chem.* **77** 1539–44
[120] He M Y, Sun C H and Chiu D T 2004 *Anal. Chem.* **76** 1222–7
[121] Oh H J, Kim S H, Baek J Y, Seong G H and Lee S H 2006 *J. Micromech. Microeng.* **16** 285–91
[122] Tan Y C, Hettiarachchi K, Siu M and Pan Y P 2006 *J. Am. Chem. Soc.* **128** 5656–8
[123] Abraham S, Jeong E H, Arakawa T, Shoji S, Kim K C, Kim I and Go J S 2006 *Lab Chip* **6** 752–6
[124] De Geest B G, Urbanski J P, Thorsen T, Demeester J and De Smedt S C 2005 *Langmuir* **21** 10275–9
[125] Barnes S E, Cygan Z T, Yates J K, Beers K L and Amis E J 2006 *Analyst* **131** 1027–33
[126] Nie Z H, Li W, Seo M, Xu S Q and Kumacheva E 2006 *J. Am. Chem. Soc.* **128** 9408–12
[127] Nie Z H, Xu S Q, Seo M, Lewis P C and Kumacheva E 2005 *J. Am. Chem. Soc.* **127** 8058–63
[128] Xu S Q, Nie Z H, Seo M, Lewis P, Kumacheva E, Stone H A, Garstecki P, Weibel D B, Gitlin I and Whitesides G M 2005 *Angew. Chem. Int. Edn* **44** 724–8
[129] Kim J W, Utada A S, Fernandez-Nieves A, Hu Z B and Weitz D A 2007 *Angew. Chem. Int. Edn.* **46** 1819–22
[130] Quevedo E, Steinbacher J and McQuade D T 2005 *J. Am. Chem. Soc.* **127** 10498–9
[131] Kim J H, Choi W C, Kim H Y, Kang Y and Park Y K 2005 *Powder Technol.* **153** 166–75
[132] Seo M, Nie Z H, Xu S Q, Mok M, Lewis P C, Graham R and Kumacheva E 2005 *Langmuir* **21** 11614–22
[133] Shepherd R F, Conrad J C, Rhodes S K, Link D R, Marquez M, Weitz D A and Lewis J A 2006 *Langmuir* **22** 8618–22
[134] Martin-Banderas L, Rodriguez-Gil A, Cebolla A, Chavez S, Berdun-Alvarez T, Garcia J M F, Flores-Mosquera M and Ganan-Calvo A M 2006 *Adv. Mater.* **18** 559

[135] Ganan-Calvo A M, Martin-Banderas L, Gonzalez-Prieto R, Rodriguez-Gil A, Berdun-Alvarez T, Cebolla A, Chavez S and Flores-Mosquera M 2006 *Int. J. Pharmaceutics* **324** 19–26
[136] Huang K S, Lai T H and Lin Y C 2006 *Lab Chip* **6** 954–7
[137] Liu K, Ding H J, Liu J, Chen Y and Zhao X Z 2006 *Langmuir* **22** 9453–7
[138] Zhang H, Tumarkin E, Peerani R, Nie Z, Sullan R M A, Walker G C and Kumacheva E 2006 *J. Am. Chem. Soc.* **128** 12205–10
[139] Zhang H, Tumarkin E, Sullan R M A, Walker G C and Kumacheva E 2007 *Macromol. Rapid Commun.* **28** 527–38
[140] Yang C H, Huang K S and Chang J Y 2007 *Biomed. Microdevices* **9** 253–9
[141] Steinbacher J L and McQuade D T 2006 *J. Polym. Sci. A Polym. Chem.* **44** 6505–33
[142] Cho S H, Jun J B, Ryu J H and Suh K D 2005 *Colloids. Surf. A* **254** 1–7
[143] Gross G A, Hamann C, Gunther M and Kohler J M 2007 *Chem. Eng. Technol.* **30** 341–6
[144] Nisisako T, Torii T, Takahashi T and Takizawa Y 2006 *Adv. Mater.* **18** 1152
[145] Dendukuri D, Tsoi K, Hatton T A and Doyle P S 2005 *Langmuir* **21** 2113–6
[146] Kubo A, Shinmori H and Takeuchi T 2006 *Chem. Lett.* **35** 588–9
[147] Jeong W J, Kim J Y, Choo J, Lee E K, Han C S, Beebe D J, Seong G H and Lee S H 2005 *Langmuir* **21** 3738–41
[148] Edmond K V, Schofield A B, Marquez M, Rothstein J P and Dinsmore A D 2006 *Langmuir* **22** 9052–6
[149] Barrero A and Loscertales I G 2007 *Annu. Rev. Fluid Mech.* **39** 89-106
[150] Euliss L E, DuPont J A, Gratton S and DeSimone J 2006 *Chem. Soc. Rev.* **35** 1095–104
[151] Yow H N and Routh A F 2006 *Soft Matter* **2** 940–9
[152] Nisisako T, Okushima S and Torii T 2005 *Soft Matter* **1** 23–7
[153] Link D R, Anna S L, Weitz D A and Stone H A 2004 *Phys. Rev. Lett.* **92** 054503
[154] Raven J P, Marmottant P and Graner F 2006 *Eur. Phys. J. B* **51** 137–43
[155] Barbier V, Tatoulian M, Li H, Arefi-Khonsari F, Ajdari A and Tabeling P 2006 *Langmuir* **22** 5230–2
[156] Okushima S, Nisisako T, Torii T and Higuchi T 2004 *Langmuir* **20** 9905–8
[157] Seo M, Nie Z H, Xu S Q, Lewis P C and Kumacheva E 2005 *Langmuir* **21** 4773–5
[158] Zheng B, Tice J D and Ismagilov R F 2004 *Adv. Mater.* **16** 1365–8
[159] Beatus T, Tlusty T and Bar-Ziv R 2006 *Nature Phys.* **2** 743–8
[160] Drenckhan W, Cox S J, Delaney G, Holste H, Weaire D and Kern N 2005 *Colloids. Surf. A* **263** 52–64
[161] Garstecki P and Whitesides G M 2006 *Phys. Rev. Lett.* **97** 024503
[162] Raven J P, Marmottant P and Graner F 2006 *Eur. Phys. J.* B **51** 137–43
[163] Hashimoto M, Mayers B, Garstecki P and Whitesides G M 2006 *Small* **2** 1292–8